

Shear-Induced Heterogeneity in Associating Polymer Gels: Role of Network Structure and Dilatancy

Ahmad K. Omar and Zhen-Gang Wang*

Division of Chemistry and Chemical Engineering, California Institute of Technology, Pasadena, California 91125, USA
(Received 8 July 2016; revised manuscript received 23 April 2017; published 12 September 2017)

We study associating polymer gels under steady shear using Brownian dynamics simulation to explore the interplay between the network structure, dynamics, and rheology. For a wide range of flow rates, we observe the formation of shear bands with a pronounced difference in shear rate, concentration, and structure. A striking increase in the polymer pressure in the gradient direction with shear, along with the inherently large compressibility of the gels, is shown to be a crucial factor in destabilizing homogeneous flow through shear-gradient concentration coupling. We find that shear has only a modest influence on the degree of association, but induces marked spatial heterogeneity in the network connectivity. We attribute the increase in the polymer pressure (and polymer mobility) to this structural reorganization.

DOI: [10.1103/PhysRevLett.119.117801](https://doi.org/10.1103/PhysRevLett.119.117801)

Associating polymers (APs) in dilute solution can aggregate into multichain clusters when the “sticker” (the physically associating moiety) attraction energy exceeds the thermal energy kT . Near the overlap concentration, sticker clusters can be bridged by polymer strands and form an interconnected volume spanning network—a physical gel [1–3]. Such gels are found in both natural and synthetic systems, and display a striking array of rheological behavior, including strain stiffening [4], negative normal stresses [5], shear thickening [6,7], shear thinning [8], and shear banding [9–15].

Despite the ubiquity and versatility of physical gels, a fundamental understanding of the interplay between their microstructure, dynamics, and rheological properties remains a challenging and open problem. For instance, while experiments and simulations of associative networks (including both AP [13–15] and colloidal [16] gels) under simple shear have observed spatial inhomogeneities in both shear rate and density, suggesting some form of shear-gradient concentration coupling (SCC) [17–20], the microscopic mechanism for the instability is unclear. Mean-field based models [21] of AP rheology have largely focused on chain elasticity and have not accounted for density inhomogeneity (e.g., chain migration) which would require a constitutive relation describing the solute pressure (the driving force for chain migration) as a function of shear rate and concentration. To date, no such relation has been explored for physical gels—largely due to the experimental difficulty in measuring the pressure of a single species in solution under shear [22]. Furthermore, the observation of SCC in both AP and colloidal gels suggests that the common physics between the gels—such as network connectivity and transient particle localization—may play a key role in driving the instability.

In this Letter, we report results from Brownian dynamics simulations of an AP gel under steady shear in the

nonlinear, shear-thinning, regime. The polymers we study have multiple associating sticker groups along the backbone, a prevalent building block of natural and synthetic gels. Our study reveals that within a broad range of applied shear rate, the gel separates into two distinct bands with substantially different shear rate and concentration. However, the applicability of existing SCC mechanisms to AP gels is unclear. While Reynolds “dilatancy,” or the tendency for increased particle pressure with shear, has been proposed as a driving force for shear-induced particle migration [22,23] and shear banding [24] in *repulsive* systems such as colloidal suspensions and glasses, the effect is marginal for dilute conditions [25]. Shear-induced turbidity in polymer [26] and wormlike micellar surfactant [27,28] solutions can be the result of a coupling of elastic stress with concentration and shear [29,30]. However, this coupling is typically more pronounced in high molecular weight, well-entangled solutions [31].

Here, we show that AP gels exhibit a significant microstructural reorganization in response to the elastic stresses due to shear. Crucially, we find the degree of association only decreases slightly with shear, but the spatial distribution of the network *connectivity* undergoes striking changes—the initial space-spanning network is broken into multiple smaller domains whose size is controlled by the shear rate. The loose connections between these distinct domains significantly enhance the polymer mobility and pressure in the gradient direction. We propose that this network “dilatation,” coupled with the inherently large compressibility (low osmotic pressure) of our gels, plays a crucial role in the observed SCC.

Our simulation system consists of 300 chains of $N = 100$ beads with 10 evenly spaced stickers along the backbone. We use a standard Kremer-Grest model to describe the chains [32]. The interaction between the nonsticker groups and between a sticker and nonsticker

is modeled by the WCA potential [33] with diameter $\sigma_{\text{LJ}} = 1$, energy $\epsilon_{\text{LJ}} = 1$, thus setting the units of length and energy, respectively. The Lennard-Jones time $\tau_{\text{LJ}} = \sqrt{m\sigma_{\text{LJ}}^2/\epsilon_{\text{LJ}}} = 1$ sets the time scale. The interaction between the stickers is a shifted LJ potential truncated at $r_c = 2.5$ with a well depth of ϵ_{ss} . The chain connectivity is described with a FENE potential using the canonical parameters (spring constant $k = 30$ and fully stretched bond length $R_0 = 1.5$). We set a Cartesian coordinate such that x , z , and y refer to the flow, gradient, and vorticity directions, respectively. We use a system box size of $V = L_x L_y L_z$ with $L_x = 10.3R_g$, and $L_y = L_z = 8.8R_g$ where $R_g \approx 6.8$ is the equilibrium radius of gyration of chains without sticker associations (hereafter referred to as Rouse chains). We impose periodic boundary conditions in the flow and vorticity directions and the Lees-Edwards boundary condition in the gradient direction [34]. The bead number density is $\bar{\rho} = 0.12$, ensuring that the solution is semidilute ($\bar{\rho} \approx 1.6\rho^*$ where ρ^* is the overlap concentration of the Rouse system).

To study larger system sizes, we ignore hydrodynamic interactions and use Langevin dynamics to evolve our system:

$$m\ddot{\mathbf{r}} = \mathbf{f}_p + \mathbf{f}_b - \zeta(\dot{\mathbf{r}} - \mathbf{r} \cdot \nabla \mathbf{v}_s), \quad (1)$$

where \mathbf{r} and \mathbf{f}_p are, respectively, the particle position and interparticle force, and the particle mass m is set at unity. The Brownian force \mathbf{f}_b is taken to be a white noise with a mean of 0 and a variance of $2kT\zeta$ where ζ is the damping coefficient. We choose $kT = 1$ and define a reduced temperature $T^* = 1/\epsilon_{ss}$ to characterize the strength of the association. The drag is with respect to the local solvent velocity with $\nabla \mathbf{v}_s = (0, 0, 0; 0, 0, 0; \dot{\gamma}, 0, 0)$ [35], where $\dot{\gamma}$ is the applied shear rate. Simulations are performed using LAMMPS [36].

We equilibrate our samples following the protocol described in the Supplemental Material [37]. The quiescent-state data are collected over a period of $190\tau_R$ (where $\tau_R \approx 1565$ is the Rouse time obtained from the diffusion data of the unassociating chains [38]). Even at the lowest T^* , chains diffuse their own size multiple times. We shear the system by using two protocols: startup shear at a constant rate for a duration of at least $250\tau_R$ and sweep with several intermediate rates for a duration of $50\tau_R$ per rate. We collect data after an initial transience; the data are averaged over at least four independent samples.

To characterize the structure of the gel, we define clusters (groups of two or more associating stickers) based on a connectivity matrix algorithm [39,40]. Stickers within a cutoff distance of 1.5 (capturing the attractive portion of the LJ potential well) are deemed associating and grouped into the same cluster. We then compute structural properties such as the network bridge (a polymer strand connecting two clusters) density n_B , the cluster functionality f (the number of bridges per cluster), and the cluster coordination

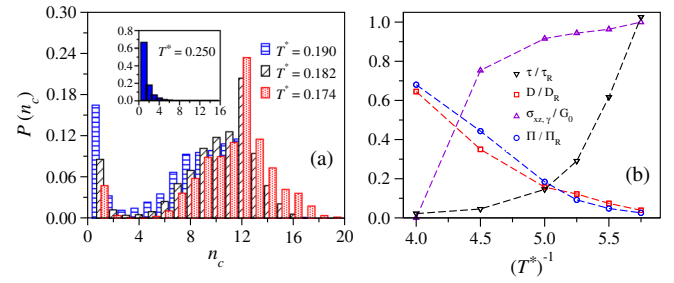


FIG. 1. Effect of T^* on (a) the weight-averaged cluster size distribution; (b) τ , D , $\sigma_{xz,y}$, and Π . The subscript R indicates properties of our Rouse system with $D_R = 6 \times 10^{-3}$ and $\Pi_R = 8.9nkT$. G_0 is the gel shear modulus at $T^* = 0.174$.

number Z_c (the number of other clusters a cluster is connected to).

We first briefly survey some key quiescent-state properties. At $T^* = 0.25$, there is little sticker aggregation; the majority of stickers remain unpaired [see inset of Fig. 1(a)]. Upon increasing the association strength to $T^* = 0.20$, the probability distribution of the cluster sizes $P(n_c)$ becomes bimodal, with a second peak emerging at larger cluster sizes. As the average cluster size increases with increasing sticker attraction, the sticker association lifetime τ (the time a sticker spends in a cluster) increases superexponentially [roughly as $\tau \propto \exp(\langle n_c \rangle / T^*)$], in agreement with the results of Kumar and Douglas [3]. As a result, the chains localize, as seen through the drop in the long-time self-diffusivity D , shown in Fig. 1(b). This “clustering transition” [3] (at $T^* = 0.22 \pm 0.02$) results in the typical rheological properties associated with the gel state. Concurrently, we find dramatic changes in the stress-strain behavior during startup shear: at a rate of $\dot{\gamma} = 10^{-4}$ ($\dot{\gamma}\tau_R < 1$), we find an initial elastic response for the APs ($\sigma_{xz,y} \equiv d\sigma_{xz}/d\gamma|_{\gamma=0} \equiv$ shear modulus and σ_{xz} is the shear stress component of the stress tensor σ and γ is the strain) only for T^* s below this transition.

The clustering of the AP chains results in a reduction of the osmotic pressure, $\Pi = -tr\sigma/3$, (and hence, osmotic modulus $\partial\Pi/\partial\bar{\rho}$) of the system. AP gels are inherently more compressible than their unassociating counterpart (which are also relatively compressible for $\bar{\rho} \sim \rho^*$). Thus, a salient feature of our AP gels is that while they become *stiffer* with increasing degrees of association in the sense that their shear modulus increases, they also become *softer* in that they are more compressible. This is a natural consequence of the proximity of the sol-gel transition boundary to the spinodal boundary [1,2].

We now turn to the steady-state behavior under shear. Starting with an AP system in the gel state, we have examined the steady-state properties for a series of shear rates, in the range of $\dot{\gamma} = 10^{-4}$ – 10^{-2} . All shear rates explored are in the nonlinear shear-thinning regime with the Péclet number $Pe \equiv \dot{\gamma}R_g^2/D > 1$. Even at the lowest shear rate, we observe the formation of shear bands for all

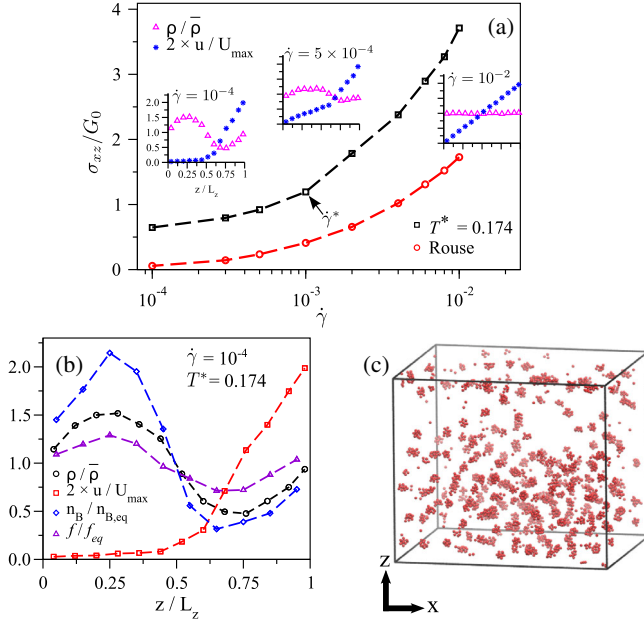


FIG. 2. (a) Constitutive curves (obtained with a combination of sweep and startup protocols) for the gel at $T^* = 0.174$ and for the Rouse solution. The insets display the AP velocity and density profiles at various shear rates. (b) Profiles for concentration ρ , velocity u ($U_{\max} = \dot{\gamma}L_z$), bridging density n_B , and cluster functionality f . The subscript “eq” denotes equilibrium properties. (c) Snapshot of banded flow (only stickers are shown for clarity).

T^* s in the gel state. At $T^* = 0.174$, bands are observed up to a shear rate of $\dot{\gamma}^* = 10^{-3}$. Interestingly, the formation of the bands is accompanied by significant concentration differences; see Fig. 2(b), where a threefold difference in concentration is shown for $T^* = 0.174$ and $\dot{\gamma} = 10^{-4}$. At this rate, the concentrated band is nearly unsheared (with an effective shear rate an order of magnitude smaller than that of the dilute phase)—a direct consequence of both the strong concentration dependence of the viscosity [8,41] and the shear stress being near the phenomenological yield stress of the band [42,43]. The significant difference in both density and shear between the bands results in a substantial spatial variation in the network structure (shown through n_B and f).

Upon increasing the rate from $\dot{\gamma} = 10^{-4}$ to $\dot{\gamma} = 5 \times 10^{-4}$, we observe that (i) the width of the bands remains relatively constant, (ii) the shear stress increases ($\sigma_{xz} - \sigma_Y \propto \dot{\gamma}^{0.75}$ where σ_Y is the material yield stress), (iii) the two bands have exchanged mass so their densities are closer (see Ref. [37] for a more quantitative measure through the structure factor), and (iv) both bands are appreciably flowing. These observations are in contrast to the constitutive-instability ($d\sigma_{xz}/d\dot{\gamma} < 0$) mechanism [17] (that has been invoked to explain the recent finding of shear bands in attractive, dense athermal (non-Brownian) particles [44]) wherein the stress and shear rates of the bands remain constant and the width of the bands increases

linearly with increasing shear [17,27]. Rather, these observations are consistent with a flow instability triggered by a strong coupling between shear and concentration [20].

Few materials have been shown to exhibit SCC instabilities in practice [24,28,42]. Phenomenologically, previous work derived the following criterion for unstable flow, by linearization of the coupled Navier-Stokes and diffusion equations with respect to density and velocity fluctuations [20,24,45]:

$$F(\bar{\rho}, \dot{\gamma}) \equiv \frac{\Pi_{zz, \dot{\gamma}} \sigma_{xz, \bar{\rho}}}{\Pi_{zz, \bar{\rho}} \sigma_{xz, \dot{\gamma}}} > 1, \quad (2)$$

where Π_{zz} is the particle pressure in the gradient direction [46] and the second subscript denotes a partial derivative with respect to that variable, e.g., $\Pi_{zz, \dot{\gamma}} \equiv \partial \Pi_{zz} / \partial \dot{\gamma}$. The terms $\Pi_{zz, \dot{\gamma}}$ and $\sigma_{xz, \bar{\rho}}$ cause particle migration towards regions of lower shear rate and increased shear rate in regions of low concentration, respectively. A local increase in particle concentration thus reduces the shear rate, promoting further particle migration. The remaining terms in Eq. (2) counteract this effect by promoting diffusive spreading of both particles ($\Pi_{zz, \bar{\rho}}$) and momentum ($\sigma_{xz, \dot{\gamma}}$).

While shear thinning and the concentration dependence of the shear stress [reflected respectively in $\sigma_{xz, \dot{\gamma}}$ and $\sigma_{xz, \bar{\rho}}$ in Eq. (2)] have been previously studied [8,41] and drive the observed large gradient in shear rate, the influence of shear on the solute pressure Π_{zz} in gels remains unexplored, in part due to the experimental difficulty in measuring this quantity [22]. In Fig. 3(a), we show the normalized deviatoric pressure $(\Pi_{zz} - \Pi_{eq})/\Pi_{eq}$ as a function of $\dot{\gamma}$ for AP gels. (For all $\dot{\gamma}$, Π_{zz} is still less than the equilibrium osmotic pressure of our Rouse system [37]). In increasing the shear rate from $\dot{\gamma} = 10^{-4}$ to $\dot{\gamma} = 10^{-3}$, Π_{zz} exhibits an increase of nearly $2nkT$ for an AP gel at $T^* = 0.174$ in comparison to $0.22nkT$ for a Rouse solution [37]. For our Rouse chains there is only weak SCC [37], insufficient to result in unstable flow for the examined shear rates. At the lower shear rates, $\Pi_{zz} \sim \Pi_{eq}$ for the AP gels, and thus the gels are nearly as compressible as in the quiescent state. This region of shear rates where the gels are highly compressible, coupled with a strong variation in Π_{zz} with $\dot{\gamma}$, is precisely where we observe a significant, sustained concentration (and shear rate) difference.

The large increase in Π_{zz} with shear in our AP gels contrasts with the known dilation [47] response of comparably dilute systems. Simulations of colloidal hard spheres at volume fractions of 10% show a pressure increase of only nkT over four decades of applied shear rate [25]. For polymer solutions, the reduction in the chain dimension in the gradient direction with shear increases Π_{zz} due to the chain elasticity. For the $\dot{\gamma}$ examined, we find no significant compression of the AP chain conformation in the gradient direction; the degree of compression is even less than our Rouse system [37], which only results in

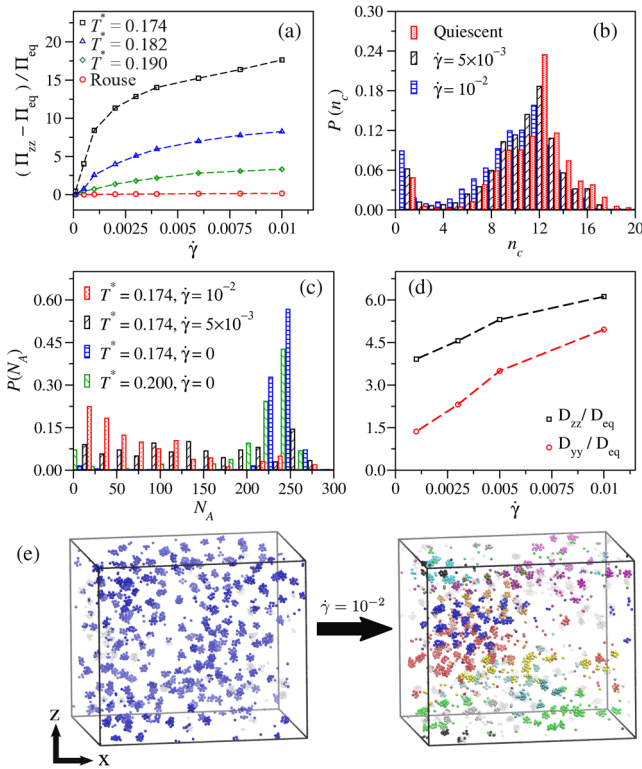


FIG. 3. (a) $(\Pi_{zz} - \Pi_{eq})/\Pi_{eq}$ as a function of $\dot{\gamma}$ and T^* . (b) Influence of $\dot{\gamma}$ on the cluster size distribution of the AP gel ($T^* = 0.174$). (c) Weight-averaged DRA size distribution (with the chains binned into groups of 20) excluding clusters with $Z_c < 4$. (d) Diffusivity in the gradient D_{zz} and vorticity D_{yy} directions in the regime of homogeneous flow. (e) Breakup of a single space-spanning DRA at equilibrium (left) to several smaller DRAs (indicated by different colors) during steady shear at $\dot{\gamma} = 10^{-2}$ (right). Stickers not belonging to a DRA are shown in grey.

modest increases in Π_{zz} with $\dot{\gamma}$. Therefore, while a contributing factor, the coupling of chain elasticity to shear does not appear to be the source of the observed SCC.

What, then, is the origin of the observed dilation? To explore this question, we focus on the structural evolution of the gel at shear rates for which the flow is homogeneous ($\dot{\gamma} > \dot{\gamma}^*$). Crucially, in this regime the density is homogeneous, allowing us to delineate the role of shear alone on the structural properties of the gel. Examination of the sticker cluster size distribution $P(n_c)$ shows a shift towards smaller aggregation with increasing $\dot{\gamma}$ [Fig. 3(b)]. From our quiescent-state analysis (cf. Fig. 1) we indeed found the pressure to increase with decreasing degree of association. However, while $P(n_c)$ appears more sensitive to T^* than $\dot{\gamma}$, raising T^* from 0.174 to 0.190 only increases the pressure by $\approx 0.6nkT$ [see Fig. 1(b)], an order of magnitude less than the pressure increases under shear. The failure to explain the significant increase in Π_{zz} with shear by introducing an effective gel temperature, suggests that the gel undergoes significant structural changes unaccounted for by shifts in $P(n_c)$.

Under steady shear, one would intuitively expect that large aggregates of connected clusters extending in the gradient direction will be subject to large elastic stresses, giving way to structural breakup. To quantify these large-scale aggregates, we extend our sticker connectivity methodology to explore the connectivity of the clusters themselves into supramolecular aggregates. Clusters that are connected by at least one polymer strand are deemed to belong to the same aggregate.

In quiescence, all of the gels explored have a single supramolecular aggregate that contains nearly all of the chains. Interestingly, even at the largest $\dot{\gamma}$, a gel at any given moment remains a space-spanning network [37]. However, some of the connections within the network are weak and undergo rapid breaking and reforming. The weakly connected regions are typically bound together by low coordination (Z_c) clusters. We therefore define a dynamically robust aggregate (DRA) to consist of clusters with $Z_c \geq 4$ (4 being the median of Z_c at equilibrium). The size distribution of the DRAs exhibits a striking qualitative change with shear as shown in Fig. 3(c). At or near equilibrium (i.e., in the linear-response regime) with $Pe \lesssim 1$, a system-spanning aggregate containing nearly all of the chains dominates the distribution, a feature that is general to APs in the gel state (the blue and green bars). Under high shear (the red and black bars) with $\dot{\gamma} > \dot{\gamma}^*$ and $Pe \gg 1$, the distribution becomes significantly broader, shifting towards smaller aggregate sizes with increasing $\dot{\gamma}$ [see Fig. 3(e) for a snapshot of the network structure under shear]. The transition between these disparate distributions is precisely the flow regime ($Pe > 1$ and $\dot{\gamma} < \dot{\gamma}^*$) where we observe the SCC instability and the significant dilatancy.

We emphasize that the difference between these distributions (e.g., see the red and green bars) is not simply a result of reduced coordination under shear, as the average coordination of the $T^* = 0.174$ gel at $\dot{\gamma} = 10^{-2}$ ($\langle Z_c \rangle = 3.4$) is larger than that of the $T^* = 0.200$ gel at rest ($\langle Z_c \rangle = 3.2$). Rather, this indicates that shear induces spatial *heterogeneity* in the network connectivity. This shear-induced heterogeneity in the network structure enhances the chain diffusivity in the gradient (and vorticity) direction [see Fig. 3(d)]. This enhanced mobility in the gradient direction, in turn, causes Π_{zz} to increase with $\dot{\gamma}$. The strong increase of Π_{zz} with $\dot{\gamma}$ at the lower shear rates, coupled with the inherently low osmotic modulus, can destabilize homogeneous flow via a SCC instability [see Eq. (2)], generating shear bands with significant dynamic and structural differences. At the low shear end of the unstable region ($\dot{\gamma} \ll \dot{\gamma}^*$ and $Pe > 1$), the low shear stress coupled with significant growth in density heterogeneity can result in the yield stress of the high-density band approaching the system shear stress, further sharpening the differences in shear (and hence density) between the bands.

In probing the mechanism of SCC in AP gels we highlight the crucial role of the mesoscale network connectivity—rather than such global measures as the degree of association—in the observed unique rheological behavior. We hope this work can inform the development of constitutive laws for the full AP stress tensor to allow for a more complete description of AP rheology. Network topology should play a similarly important role in determining the mechanical (beyond elasticity) and dynamical properties of AP solutions and gels at equilibrium. We leave the theoretical elucidation of this role to future work.

We thank John Brady and Marco Heinen for fruitful discussions. A. K. O. acknowledges support by the National Science Foundation Graduate Research Fellowship under Grant No. DGE-1144469 and an HHMI Gilliam Fellowship.

*zgw@caltech.edu

- [1] A. N. Semenov and M. Rubinstein, *Macromolecules* **31**, 1373 (1998).
- [2] S. K. Kumar and A. Z. Panagiotopoulos, *Phys. Rev. Lett.* **82**, 5060 (1999).
- [3] S. K. Kumar and J. F. Douglas, *Phys. Rev. Lett.* **87**, 188301 (2001).
- [4] C. Storm, J. J. Pastore, F. C. MacKintosh, T. C. Lubensky, and P. A. Janmey, *Nature (London)* **435**, 191 (2005).
- [5] P. A. Janmey, M. E. McCormick, S. Rammensee, J. L. Leight, P. C. Georges, and F. C. MacKintosh, *Nat. Mater.* **6**, 48 (2007).
- [6] S. Suzuki, T. Uneyama, T. Inoue, and H. Watanabe, *Macromolecules* **45**, 888 (2012).
- [7] G. Ianniruberto and G. Marrucci, *Macromolecules* **48**, 5439 (2015).
- [8] T. Annable, R. Buscall, R. Ettelaie, and D. Whittlestone, *J. Rheol.* **37**, 695 (1993).
- [9] J. Billen, M. Wilson, and A. R. Baljon, *Chem. Phys.* **446**, 7 (2015).
- [10] K. A. Erk and K. R. Shull, *Macromolecules* **44**, 932 (2011).
- [11] K. A. Erk, J. D. Martin, Y. T. Hu, and K. R. Shull, *Langmuir* **28**, 4472 (2012).
- [12] T. L. Thornell, B. A. Helfrecht, S. A. Mullen, A. Bawiskar, and K. A. Erk, *ACS Macro Lett.* **3**, 1069 (2014).
- [13] J. Sprakel, E. Spruijt, M. A. Cohen Stuart, N. A. M. Besseling, M. P. Lettinga, and J. van der Gucht, *Soft Matter* **4**, 1696 (2008).
- [14] J. Sprakel, E. Spruijt, J. van der Gucht, J. T. Padding, and W. J. Briels, *Soft Matter* **5**, 4748 (2009).
- [15] J. Castillo-Tejas, S. Carro, and O. Manero, *ACS Macro Lett.* **6**, 190 (2017).
- [16] J. Colombo and E. Del Gado, *J. Rheol.* **58**, 1089 (2014).
- [17] J. K. G. Dhont and W. J. Briels, *Rheol. Acta* **47**, 257 (2008).
- [18] S. M. Fielding, *Rep. Prog. Phys.* **77**, 102601 (2014).
- [19] P. Nozières and D. Quemada, *Europhys. Lett.* **2**, 129 (1986).
- [20] V. Schmitt, C. M. Marques, and F. Lequeux, *Phys. Rev. E* **52**, 4009 (1995).
- [21] F. Tanaka and S. Edwards, *J. Non-Newtonian Fluid Mech.* **43**, 247 (1992); A. Tripathi, K. C. Tam, and G. H. McKinley, *Macromolecules* **39**, 1981 (2006); M. K. Sing, Z.-G. Wang, G. H. McKinley, and B. D. Olsen, *Soft Matter* **11**, 2085 (2015).
- [22] A. Deboeuf, G. Gauthier, J. Martin, Y. Yurkovetsky, and J. F. Morris, *Phys. Rev. Lett.* **102**, 108301 (2009).
- [23] P. R. Nott and J. F. Brady, *J. Fluid Mech.* **275**, 157 (1994).
- [24] R. Besseling, L. Isa, P. Ballesta, G. Petekidis, M. E. Cates, and W. C. K. Poon, *Phys. Rev. Lett.* **105**, 268301 (2010).
- [25] Y. Yurkovetsky and J. F. Morris, *J. Rheol.* **52**, 141 (2008).
- [26] M. Cromer, M. C. Villet, G. H. Fredrickson, and L. G. Leal, *Phys. Fluids* **25**, 051703 (2013).
- [27] S. Fielding and P. Olmsted, *Eur. Phys. J. E* **11**, 65 (2003).
- [28] M. E. Helgeson, L. Porcar, C. Lopez-Barron, and N. J. Wagner, *Phys. Rev. Lett.* **105**, 084501 (2010).
- [29] E. Helfand and G. H. Fredrickson, *Phys. Rev. Lett.* **62**, 2468 (1989).
- [30] X.-L. Wu, D. J. Pine, and P. K. Dixon, *Phys. Rev. Lett.* **66**, 2408 (1991).
- [31] S. T. Milner, *Phys. Rev. Lett.* **66**, 1477 (1991).
- [32] K. Kremer and G. S. Grest, *J. Chem. Phys.* **92**, 5057 (1990).
- [33] J. D. Weeks, D. Chandler, and H. C. Andersen, *J. Chem. Phys.* **54**, 5237 (1971).
- [34] A. W. Lees and S. F. Edwards, *J. Phys. C* **5**, 1921 (1972).
- [35] In reality, the solvent velocity field will evolve as momentum is exchanged with the solute. The solvent stress (or flow profile) is coupled to the shear stress of the solute through the hydrodynamic drag. As such, our simulations likely provide a conservative estimate for the SCC effects as the assumed solvent drag in the Langevin equation of motion [Eq. (1)] acts as a homogenizing force on the polymer flow profile.
- [36] S. Plimpton, *J. Comput. Phys.* **117**, 1 (1995).
- [37] See Supplemental Material at <http://link.aps.org/supplemental/10.1103/PhysRevLett.119.117801> for details of the equilibration protocol, calculation methods, structure factor as a function of shear, further discussion of the polymer pressure, and a visual comparison of different connectivity criteria.
- [38] M. Doi and S. F. Edwards, *The Theory of Polymer Dynamics* (Oxford University Press, New York, 1986).
- [39] E. M. Sevick, P. A. Monson, and J. M. Ottino, *J. Chem. Phys.* **88**, 1198 (1988).
- [40] M. Surve, V. Pryamitsyn, and V. Ganesan, *Phys. Rev. Lett.* **96**, 177805 (2006).
- [41] M. Rubinstein and A. N. Semenov, *Macromolecules* **31**, 1386 (1998).
- [42] H. Jin, K. Kang, K. H. Ahn, and J. K. G. Dhont, *Soft Matter* **10**, 9470 (2014).
- [43] P. C. F. Møller, S. Rodts, M. A. J. Michels, and D. Bonn, *Phys. Rev. E* **77**, 041507 (2008).
- [44] E. Irani, P. Chaudhuri, and C. Heussinger, *Phys. Rev. Lett.* **112**, 188303 (2014).
- [45] M. Cromer, G. H. Fredrickson, and L. G. Leal, *Phys. Fluids* **26**, 063101 (2014).
- [46] Assuming normal stress differences to be negligible, others (see Refs. [23,24]) have presented Eq. (2) in terms of the isotropic particle pressure Π rather than the normal pressure in the gradient direction Π_{zz} .
- [47] J. D. Ferry, *Viscoelastic Properties of Polymers* (Wiley, New York, 1980).